# Investigation of the Uncertainty of a Validation Experiment due to Uncertainty in its Boundary Conditions

Jeff Harris, David Nani, Kyle Jones, Mohanad Khodier, Barton L. Smith Utah State University

#### Abstract

Elements contributing to uncertainty in experimental repeatability are quantified for data acquisition in a bank of cylinders. The cylinder bank resembles the lower plenum of a high temperature reactor with cylinders arranged on equilateral triangles with a pitch to diameter ratio of 1.7. The 3-D as-built geometry was measured by imaging reflections off the internal surfaces of the facility. This information is useful for building CFD grids for Validation studies. Time-averaged Particle Image Velocimetry (PIV) measurements were acquired daily over several months along with the pressure drop between two cylinders. The atmospheric pressure was measured along with the data set. The PIV data and pressure drop were correlated with atmospheric conditions and changes in experimental setup. It was found that atmospheric conditions play little role in the channel velocity, but impact the pressure drop significantly. The adjustments made to the experiment setup did not change the results. However, in some cases, the wake behind a cylinder was shifted significantly from one day to the next. These changes did not correlate with ambient pressure, room temperature, nor tear down/rebuilds of the facility.

# 1 Introduction

This paper will discuss two issues of importance to computational fluid dynamics (CFD) validation experiments: as-built geometries and non-repeatability. Each of these will be explored using the same facility—a confined cylinder array.

Simulation methods, such as CFD, are essential tools in engineering design. In the case of nuclear safety, improved CFD models can significantly increase the understanding of failure and accident scenarios. The growth of CFD for nuclear applications is evident from publications, both in journals and conferences, where CFD is shown to be a common tool used in nuclear reactor design and safety analyses. However, relying on CFD as the primary source of safety analysis requires validation of the codes and models. The importance of numerical model validation is understood and has generated the important field of Verification and Validation (V&V).

For CFD to be useful, the CFD calculations, including the models used, e.g., for simulating turbulence, heat transfer, multiphase flow, chemical reactions, etc., must be validated against experimental data to ensure the level of accuracy needed and expected for their intended use.

Herein, we use the methodology described by Oberkampf and Roy [1], where a complete system is divided into several tiers. Each tier has several components that can be made into separate experiments. To validate a model of the complete system, experiments must be done on every tier and each upper level tier is validated by the experiments below it. The experiment performed for this paper fits into a benchmark tier, the third division in [1], where the boundary conditions are simple and the geometry is a simplified section of the complete system. Several features of experimental data are expected to be measured for a validation study in this tier and they include:

- 1. Detailed inspection of all hardware
- 2. Characterization of the variability of materials used in the experiment
- 3. Detailed information concerning assembly of the hardware
- 4. Detailed measurement of boundary conditions and excitation that were produced by the experimental apparatus or testing equipment

To achieve the geometric part of the hardware inspection, we have developed a technique and software for measuring the internal dimensions of a transparent facility. Software that will recognize standard shapes (straight walls and cylinders) while ignoring dust and scratches is described. When complete, this software will deliver the coordinates of the inner surface of a facility in three dimensions that can be input to solid modeling software.

The second point and the last point in the list above include an uncertainty analysis for the experiment. Any experiment contains variability, which includes the variability of atmospheric conditions and experimental setup. A major result presented in this paper is that the time-scales of these variations can have an extremely large range, and that the variations can be caused by both experimental changes as well as sources that cannot be identified. We will demonstrate this by repeating an experiment in a cylinder array dozens of times. In some cases, nothing is changed, while in others, the setup is changed in a way that one would like to believe will not change the result. We will show that the typical precision uncertainty estimate of the uncertainty of the mean of a quantity based on a single data set can be misleading when describing the overall uncertainty of the measurement.

# 2 Description of the Experiment

The cylinder array used for both the non-repeatability study and the as-built geometry study will be discussed. The model is the same for both experiments, but the setup for the measurements is different.

#### 2.1 Cylinder Array Model

The cylinder array, which was built to resemble the lower plenum of a high temperature reactor, has previously been used for validation studies [2, 3, 4]. We presently aim to learn about experimental parameters that are commonly assumed to be insignificant but that may affect the results. The parameters considered are ambient conditions (pressure, temperature and humidity), the measurement location, the camera field of view, and the small movements in the camera position that could result from every-day lab use and removing the lens cap.

With the experiment in a fixed setup (laser and camera in a fixed position; we will refer to this the baseline case), data were acquired daily as the atmospheric pressure, and other, unmeasurable factors, changed. Daily changes in the velocity and pressure drop downstream of cylinder 4 and atmospheric pressure (which changed daily) were recorded. The room temperature was constant day to day.

During the several months of data acquisition, days were selected to move the camera or the laser to four other positions (with the atmospheric pressure constant and the other optical components in the baseline position). Data were collected at five camera positions and were acquired while other parameters (atmospheric pressure, laser position, experimental setup, etc) were constant. This effectively alters the magnification of the PIV measurement. The same procedure was repeated with the laser at different positions while the camera was fixed at the baseline position. This alters the spanwise measurement location.

Figure 1: The facility used in this study. Air enters through screens at the left, into a contraction and into the test section. The field of view for the PIV data is shown (i.e. the laser sheet). The laser sheet moves through the near transparent side of the facility and cylinder and terminates on the opaque far side. Streamwise locations of the pressure taps are indicated with arrows on the top wall. These taps are in the spanwise center of the channel.

A common assumption in PIV measurements is that the optical setup remains fixed day to day when no deliberate changes have been made to it. To learn if small changes from lens cap removal and other factors were significant, the data from each day was processed with the same calibration. The data were then reprocessed with a calibration specific to that data set (based on the known channel width).

The experimental model consists of three sections shown in Fig. 1: inlet contraction, test section, and an outlet which connects to the downstream blower. The inlet has a 1.4:1 contraction in the span-wise direction and a 3:1 contraction in the cross-stream direction. Turbulence within the facility is controlled at the inlet by a single bank of 112 wires/cm screen. Flow leaving the test section is drawn through two perforated plates oriented perpendicular to the flow and inside the outlet. The perforated plates suppress separation and pulsations generated by the blower. The frequency controlled centrifugal blower is located downstream of the outlet, connected to the outlet by flexible duct, and draws atmospheric air through the facility.

The test section is a channel L= 89.7 cm in the stream-wise direction (x), w= 8.53 cm in the cross-stream direction (y), and H= 34.8 cm in span-wise direction (z). The channel contains an array of cylinders and half-cylinders (D=5.03 cm) which resembles an infinite array of cylinders arranged on equilateral triangles. Five center cylinders are placed on the cross-stream centerline with a stream-wise distance of 14.8 cm between cylinders. Each of the cylinders have a different surface finishing. Using Fig. 1 as a reference, the fourth cylinder is made from three polished polycarbonate tubes, providing measurement access to the back side of the cylinder. These three pieces are joined with aluminum disks to form a single, continuous cylinder. Center cylinder one is finished with a flat black spray paint, while center cylinders two, three, and five are coated in rhodamine dye applied using a spray. Four sets of half-cylinders are placed directly between the centerline cylinders on the cross-stream edges. All of the bottom and top half cylinders are coated in the same rhodamine dye as those of the centers. Additional details on the experimental model may be found in [2]. The velocity and property values measured in this study based on local barometric pressure are  $\rho = 1.014 \pm 0.00325 \text{kg/m}^3$ ,  $\mu = 1.82 \times 10^{-5} \pm 1.94 \times 10^{-8} \text{kg/m}$ -s and  $U_{\text{max}} = 14.3 \pm 0.6 \text{ m/s}$ .

Velocity measurements were obtained using particle image velocimetry (PIV) consisting of a high speed system from LaVision. The system was composed of a 10-bit,  $1024 \times 1024$  pixel Fastcam CMOS high speed camera and a Photonics ND:YLF 20 mJ single cavity laser. Both systems were controlled with DaVis 7.2 from LaVision [5]. Seeding for the PIV was performed using oil droplets that entered the test section at the inlet. Images were processed with deformed interrogation regions with an initial window size of  $32\times32$  and with two consecutive passes at  $16\times16$  using a 2D Standard Cross Correlation algorithm. All interrogation regions were overlapped by 50%. Results were then post-processed using

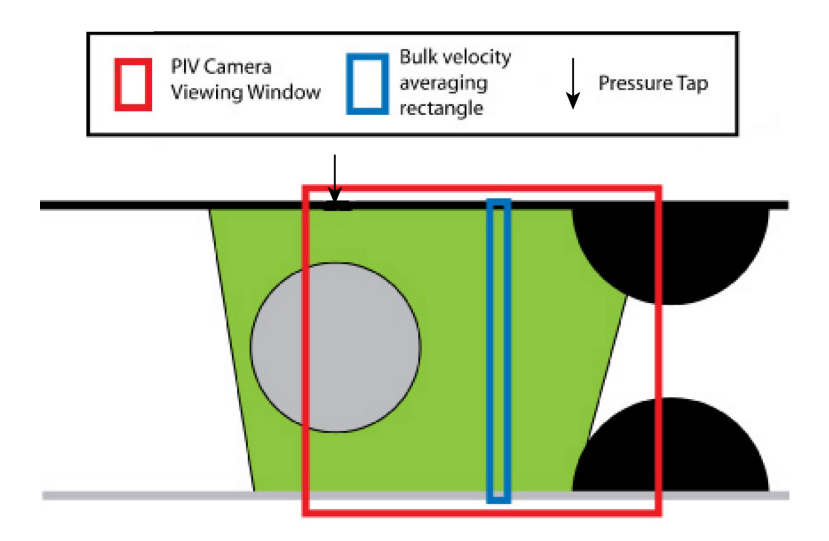


Figure 2: The view from the PIV camera. The laser sheet enters from the bottom of the figure through the clear wall and stops at the black wall at the top of the figure. The red box shows the camera viewing window and the blue box shows the area used to average the bulk velocity. The black arrow shows where the downstream pressure tap is located (see also Fig. 1).

four parameters [5]: an allowable pixel range (vectors displacing more than 15 pixels are rejected), correlation peak ratio, neighboring vectors median filter, and small groups (spurious vectors in groups smaller than 5 vectors are thrown out).

Velocity measurements were made downstream of the fourth cylinder on the x-y plane (the downstream measurement plane for cylinder 3 is shown in Fig. 2). The laser sheet entered the facility from the transparent polycarbonate cross-stream side and was terminated on the far opaque side. The high speed laser and camera could each be traversed independently along the span (z direction) of the facility.

The laser position was fixed 1 inch below the span wise center of the channel. The camera was fixed at a position 0.5 inch above the lowest point possible with the field of view provided by the optics. At this position, data were acquired daily to determine if the atmospheric pressure (or other, unknown factors) altered the velocity and pressure results. In a separate set of measurements, the camera and laser were reposition to either move to a different span wise location or to change the magnification of the measurement.

At the highest laser position, the camera could be at the lowest position and still capture the width of the channel. The laser sheet was placed at the center of the channel in a position is referred to as 0. The laser was moved down at 0.5-inch increments with the camera at the 0.5-inch position. The camera was moved from 0 to 2 inches in 0.5 inch increments with the laser fixed at -1 inch. To determine the effect that the movement of the laser and camera have on experimental results, five PIV and pressure drop data sets were recorded in one day (so that the atmospheric pressure was constant). On one day, the camera would be moved and the laser would stay fixed. On another day, the laser would be moved and the camera would stay fixed. Then both camera and laser would be returned to 0.5 inch and -1 inch respectively for the next daily data acquisition.

The PIV camera was always focused just behind cylinder 4, as shown in Fig. 2. The view from the camera and the rectangle used to find the bulk velocity are also shown Fig. 2. The rectangle for averaging the bulk velocity had a left side position of 12 mm from the tip of the gray, upstream

cylinder. The rectangle was 2 mm wide (so the right side was at 14mm from the upstream cylinder). The velocity profiles were found in the center of the bulk velocity rectangle (at position 13 mm from the upstream cylinder).

Pressure taps of diameter 1.59 mm were drilled into the back wall of the facility (shown by arrows in Fig. 1). All taps were placed at the spanwise centerline and were at the same streamwise position as the axis of the full cylinders 3 and 4. The pressure measurements were made using an MKS Baratron pressure sensor with 1 Torr range. The MKS Type 270D signal conditioner was used to read the sensor. The pressure data were acquired from the signal conditioner through the data acquisition system from National Instruments. During the 36 seconds of PIV data acquisition, 2160 pressure readings were recorded and averaged.

### 2.2 As-Built Geometry

Our aim is to estimate the as-built dimensions and their uncertainty for transparent geometries illuminated by a laser sheet and imaged by a camera. An experiment was designed to image the cylinder array facility using a camera with an 108-mm lens illuminated by an Nd:YAG laser. Because the illumination of the laser on the cylinder edges casts a shadow due to the top row of half cylinders, the experiment was conducted in two parts: one with the center and bottom row of cylinders relative to the camera and laser, and another with the top and bottom row of cylinders. An example of inverted images is shown in Fig. 3. In Fig. 3 a), the first phase is shown with the only the center and bottom cylinders visible. In Fig. 3 b), the second phase is represented with only the top and bottom cylinders visible. The bottom row of half cylinders are included in each phase to use as a splicing point for adjacent sets of data, since the entire facility could not be viewed by the camera. Note that the laser was positioned directly above the center cylinder for the first phase of the experiment, and then mounted at a 45 degree angle from the top to better illuminate the top row of cylinders. The array was mounted onto two traverses set up to allow the array to translate in a two-dimensional plane. During data acquisition, the cylinders were translated into or away from the view of the camera in order to make measurements along the span. Images were acquired in 2-mm increments down the length of the cylinder. The system was controlled and the data acquired using LabVIEW. The cylinders in this experiment each have different surface finishes, as described in section 2.1. 60 images were taken at each location down the span of the cylinder array to reduce random uncertainty.

The resulting images were processed in MATLAB. The computer algorithm requires two selected starting points as input from the user to locate a cylinder or edge. This comes from a command prompt to click on an image in the MATLAB environment, and the points selected are along the illuminated portion of the cylinder with the intent to cover as much of the edge as possible. The image is then processed using MATLAB built-in functions. The image processing can be described in two phases. The first uses a binary intesity conversion of the image to obtain a rough estimate of the cylinder dimensions. MATLAB functions are available to trace boundaries of binary information, and return (x,y) coordinates of each pixel along that boundary. Applying a least-squares fit of these points for the equation of a circle returns the radius and center coordinates of the circle. The second phase uses the rough estimate of the radius and center coordinate location of the cylinder circle to find the intensity profile of the illuminated band. The intensity profiles were all perpendicular to the solid edge, and were spaced one pixel. The profiles were also taken to be 40 pixels wide to ensure that the bright pixels fell inside the interrogation region. The pixel with the maximum intensity is taken to be the solid edge and that coordinate location was recorded. Applying this to the entire edge gave points suitable for a least-squares fit to again find the radius and center coordinates of the circle for each of the cylinders, and a similarly to find the slope and intercept of the straight edges. Fig. 4 is a graphic of examples of the intensity profiles for each of the three types of finishes investigated in this experiment: flat black, rhodamine, and polycarbonate. The intensities are on a grayscale where the highest value is white and

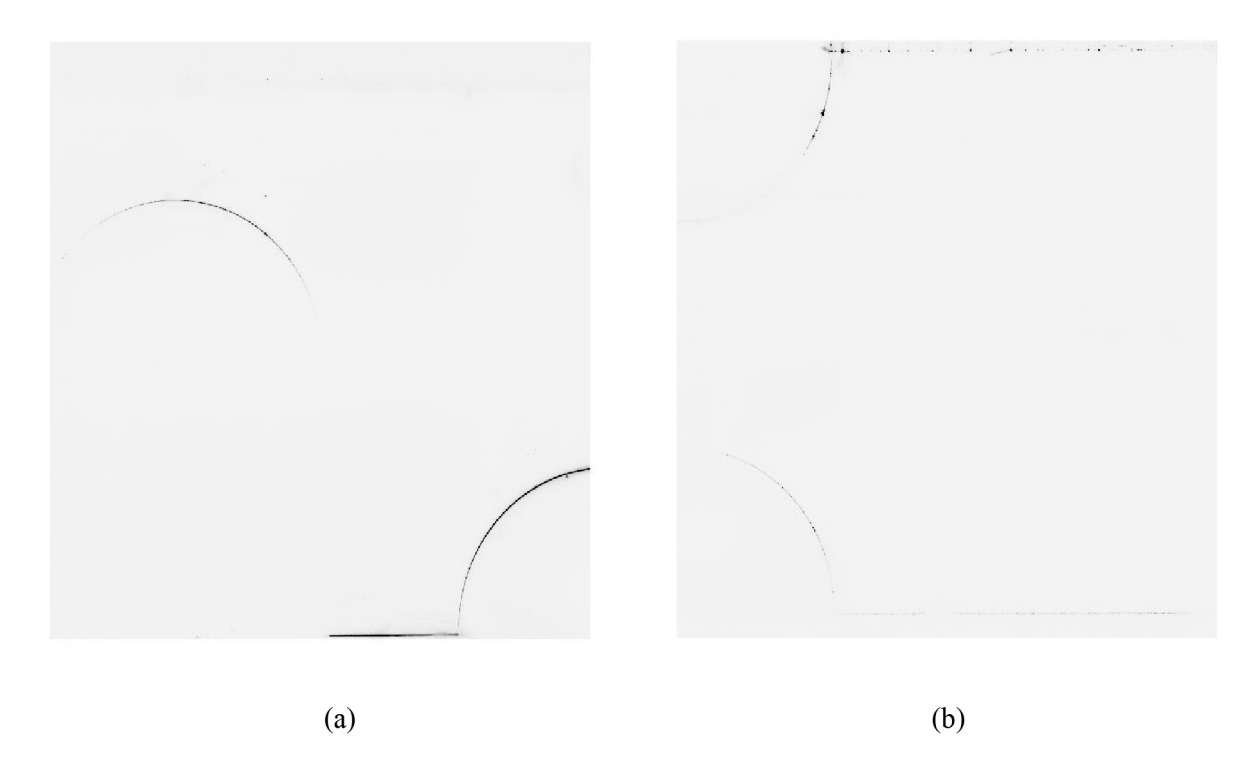


Figure 3: An inverted image of a portion of the cylinder array facility. Visible in the image are the front, top and bottom walls as well as, a) about a quarter of the center and bottom cylinders, and b) about a quarter of the top and bottom cylinders.

the lowest is black. The flat black finish shows a low intensity profile while the polycarbonate shows a high profile.

Note that the fit applied in obtaining these dimensions was tested for propagated uncertainty from the pixels measured in the images to a useful dimension. A bias uncertainty of one pixel due to the camera resolution of  $1012 \times 1008$  pixels and the 60 images taken at each location as a basis for random uncertainty were assumed. The Monte Carlo method was employed to find that the built-in MATLAB function which performs the fit yields propagated uncertainty on the order of  $10^{-13}$  pixels. This instilled confidence in employing this method to obtain accurate results.

One of the ultimate goals of this work is to use the optical measurements to complete a solid model with dimensions "as built" of the actual facility. With the radius and coordinate center locations of each cylinder of the array 2 mm apart down the cylinder length, the MATLAB program was written to fit a set of coordinate points  $\pi/50$  radians apart, representing the cylinder edges, into a text file. This text file was then imported into ANSYS software package Gambit. This was done because of the availability and ease of turning vertex data into faces and then volumes. Once Gambit had each cylinder in the form of a volume, a mesh could be generated to be used in computational fluid dynamics (CFD) simulations.

## 3 Results and Discussion

#### 3.1 Repeatability and Atmospheric Pressure

The effect atmospheric pressure had on the results was found by acquiring data daily. As shown in Fig. 5a, the bulk velocity had much higher relative variation day to day than the atmospheric pressure.

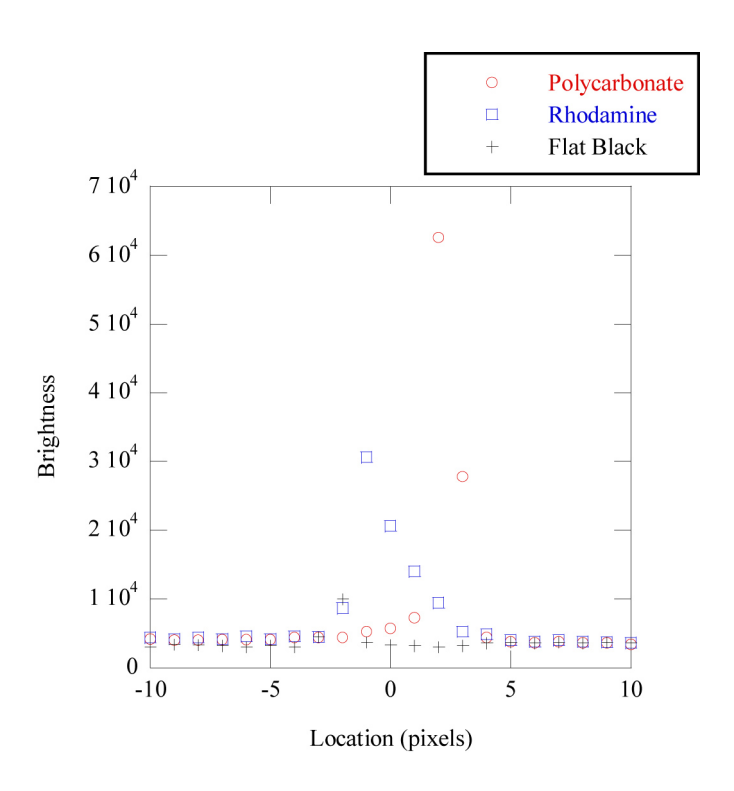


Figure 4: Intensity profiles on a grayscale of the three types of finishes used in this experiment: flat black, rhodamine, and polycarbonate (transparent). The locations are the arbitrary pixel locations the intensity bands were taken from.

The changes appear somewhat correlated, but it is clear that the changes in ambient pressure are not large enough to explain the large day-to-day variations in the bulk velocity.

Fig. 5b shows that the pressure drop between two cylinders also changes day to day, and that these changes are not correlated to the variations in the bulk velocity. Fig. 5 shows the limits of repeatability for this experiment and that the non-repeatability is not due to any quantity that we have controlled or measured.

#### 3.1.1 Velocity Profiles

The velocity profile behind cylinder 4 was monitored day to day. Several data sets coincidentally had the same barometric pressure and the resulting velocity profiles were computed. Fig 6 shows the profiles at or very near a nominal barometric pressure (640 mmHg). The velocity profile has significant variation even when the barometric pressure remains constant. Several other profiles are shown in Fig. 7a (with varying barometric pressure). The profiles show considerable variation day to day, even when no controllable factors were adjusted. Also, the data acquired on March 10 show a substantially different behavior than the rest, with the wake moving closer to the right hand wall. This shift does not correlate to any changes in atmospheric conditions nor tear down/rebuild of the channel. After March 10, the profiles returned to the left hand side for the majority of the experiments. There were, however, several cases where the mode was on the side shown by the March 10 profile.

The precision uncertainty for the mean velocity for a single data set (e.g. the data acquired on February 24, consisting of 1024 vector fields) was computed with 95% confidence. The precision uncertainty was then compared to the uncertainty found from the statistics of all of the profiles combined (repeatability uncertainty). Using all of the daily profiles, a mean profile with repeatability uncertainty bands was found and is shown in Fig. 7b. The magnitude of the uncertainty bands in

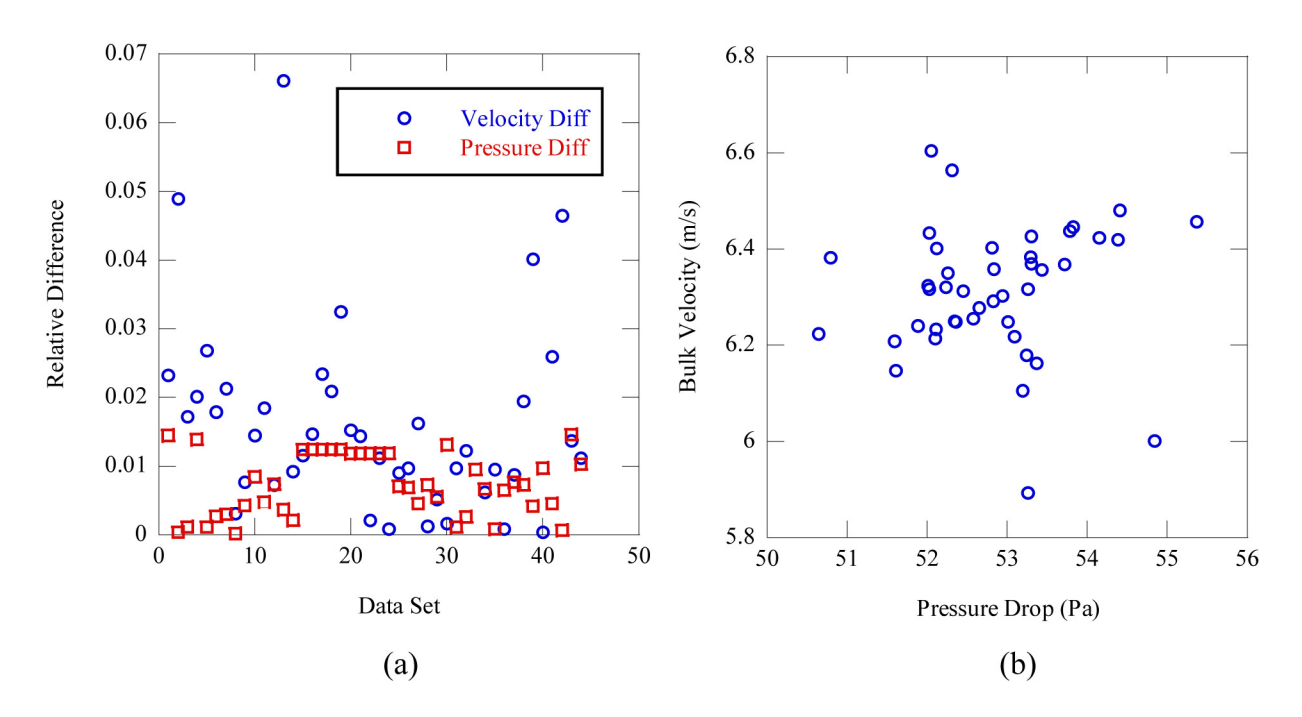


Figure 5: (a) The relative difference of the atmospheric pressure and the bulk velocity. The percent difference is computed using the mean of the pressure and the mean of the bulk velocity over several weeks of data. The mean pressure was 641.43 mmHg and the mean velocity was 6.31 m/s. (b) The bulk velocity in the channel as a function of pressure drop. It is seen that for a certain pressure drop, there were a wide range of bulk velocities.

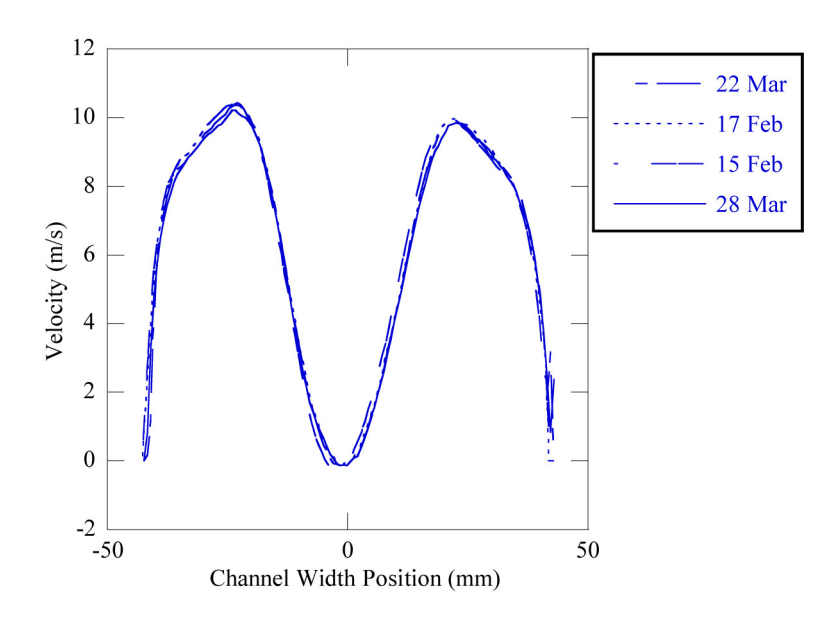


Figure 6: Several velocity profiles are shown. 22 Mar, 17 Feb, and 15 Feb are at the same barometric pressure. The other is within  $0.2~\mathrm{mmHg}$  (0.03%).

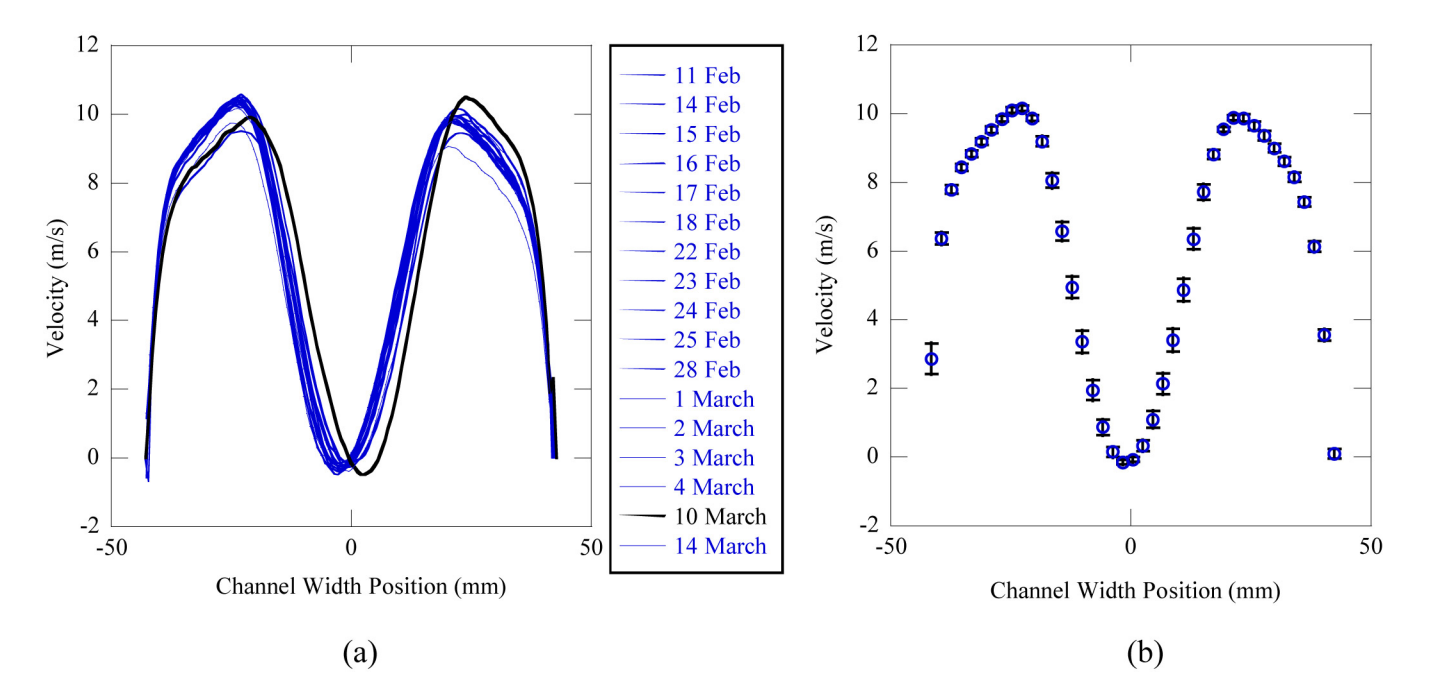


Figure 7: (a) The daily velocity profiles measured just downstream of cylinder 4. All of the profiles are in the left mode except the March 10 trace (shown in black). (b) The average velocity profile measured just downstream of cylinder 4 with uncertainty bands based on statistics taken from the daily average profiles.

Fig. 7b were found by computing the standard deviation point by point in the profiles and computing the uncertainty with 95% confidence.

Fig. 8 shows the difference between the repeatability uncertainty and the precision uncertainty of a single day's profile. Generally, the precision uncertainty of a single day is slightly higher than the repeatability uncertainty (shown by negative values in Fig 8). The exceptions are near the channel walls and in the middle of the channel (just behind cylinder 4). The middle section shows that the variation in the mode of the wake makes the repeatability uncertainty more significant than in other areas of the profile. Since the mode of the wake is not a controllable aspect of the flow, it introduces a significant repeatability uncertainty. Both the repeatability and precision uncertainties have nearly the same magnitudes. The dominating uncertainty does change through the profile, showing that neither uncertainty alone can quantify the overall uncertainty of the velocity profile.

#### 3.1.2 Camera/Laser Movement

The movement of the laser and camera, which changed the measurement location and/or the number of vectors in the profile, did generate significant change in the velocity profiles (the pressure drop is independent of the PIV system position). Fig. 9 shows the profiles for the various camera and laser positions. All of the profiles are in the same mode, but have varying magnitude. The profiles were taken within minutes of one another, so the change in the velocity profile cannot be fully attributed to changes in atmospheric conditions. Movement of the laser created variations in the velocity profile results (a different plane in the test section). The camera position variations changed the number of vectors in the cross-stream profile (different magnifications of the viewing window). As the camera position was increased (moved away from the test section), the number of vectors in the profile decreased. This caused increased variation in the profile when compared to the laser movement profiles. Both camera and laser movements changed the velocity profile, with the camera movement being more significant

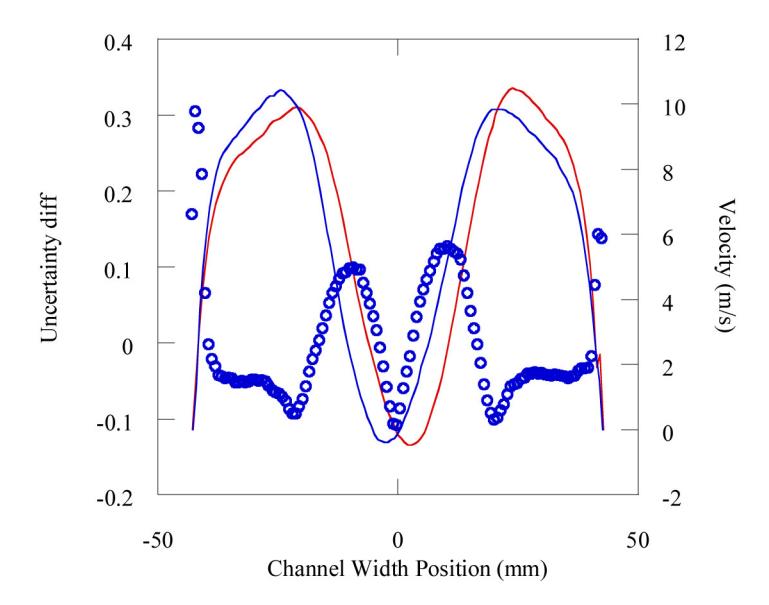


Figure 8: The uncertainty of the ensemble average profile subtract the precision uncertainty of the Feb. 24 data. Positive values mean that the repeatability uncertainty is higher than the single data set's uncertainty. Two velocity profiles are included for comparison on the secondary axis (one profile for both observed modes of the wake).

than the laser movement.

#### 3.1.3 Non-deliberate Camera Movement

Each data set was first processed assuming that the camera position and magnification was the same each day. The calculation was then repeated using a calibration computed for each data set. The bulk velocities found from the two different computations for each data set are plotted in Fig. 10. A difference of 0.1 m/s is nearly constant throughout the data. This does not show that removing the lens cap and other similar factors contribute to variation in the bulk velocity. There is however, one data set that changes more than the others when processed separately (point 8 in Fig. 10).

#### 3.2 As-Built Results

Optical and actual (direct) measurements of the cylinders are shown graphically in Fig. 11 (a) and (b). The polycarbonate cylinder is number 4 (Fig.1) and has the most error. The maximum intensity is taken to be the cylinder edge, and the variance is due to reflection in the cylinder. Also, the aluminum splicing disks used to join the polycarbonate sections reflect more than the cylinder itself, which is evident in the data peaks in Fig. 11 (a). Lastly, the general trend of the polycarbonate measurements are above their actual measurements, indicating the light reflects outward from the cylinder. The rest of the data yielded more consistent results.

The fifth cylinder is uniquely painted flat black, and the data trend is more smooth and measures slightly more than the actual dimension. The remaining rhodamine dye-painted cylinders were generally measured slightly smaller than the actual dimensions for the center cylinders and slightly larger than the actual dimensions for the bottom cylinders. The data peaks in these other sets are due to random reflections from the acrylic front wall and flat black painted back wall of the facility. Both of these surfaces had some scratches that reflected the light which would interfere with the code's ability to locate the intensity profiles accurately. This is why these data peaks generally occur near the front or back of the depth of the cylinder array.

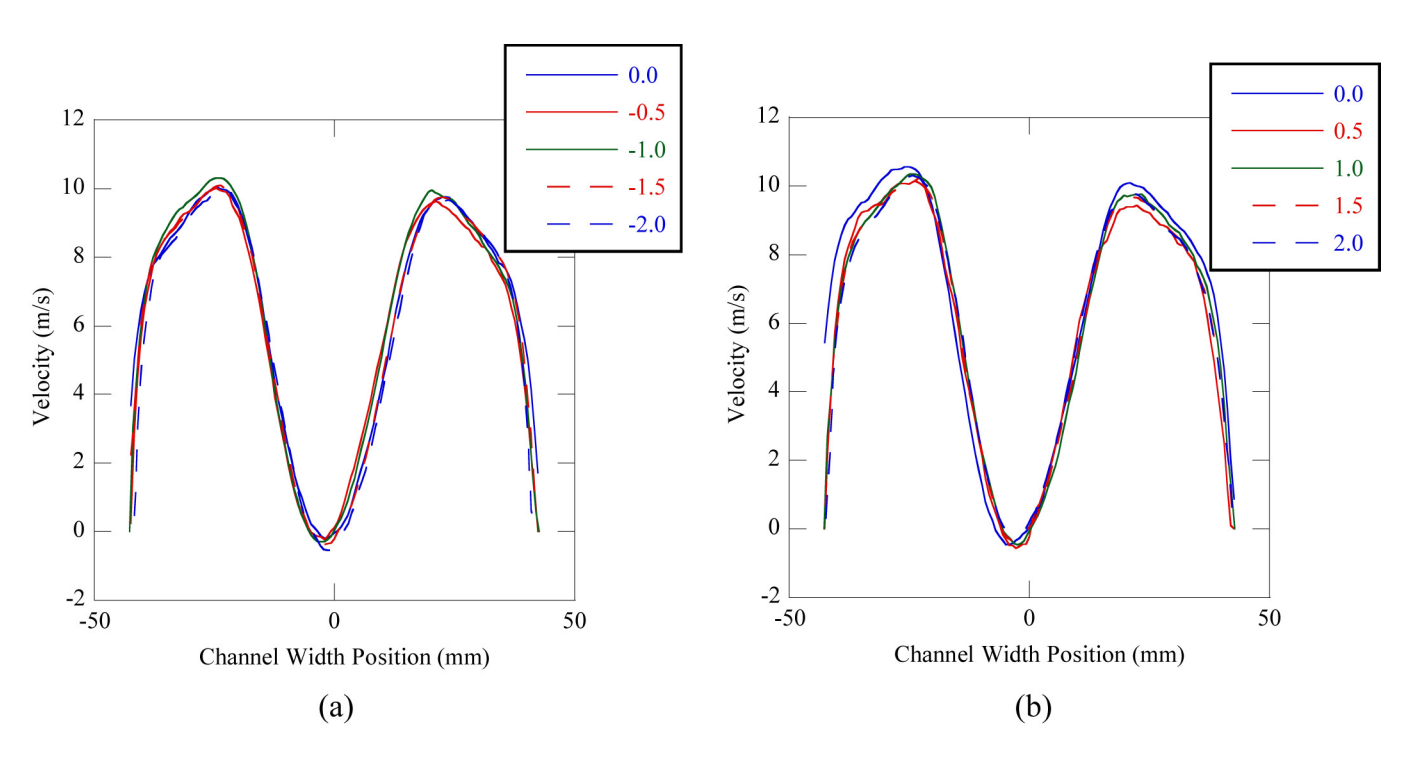


Figure 9: The velocity profiles measured just downstream of cylinder 4 for the laser positions (a) and the camera positions (b). In (a), the camera was held at a constant position and in (b) the laser was held at a constant position.

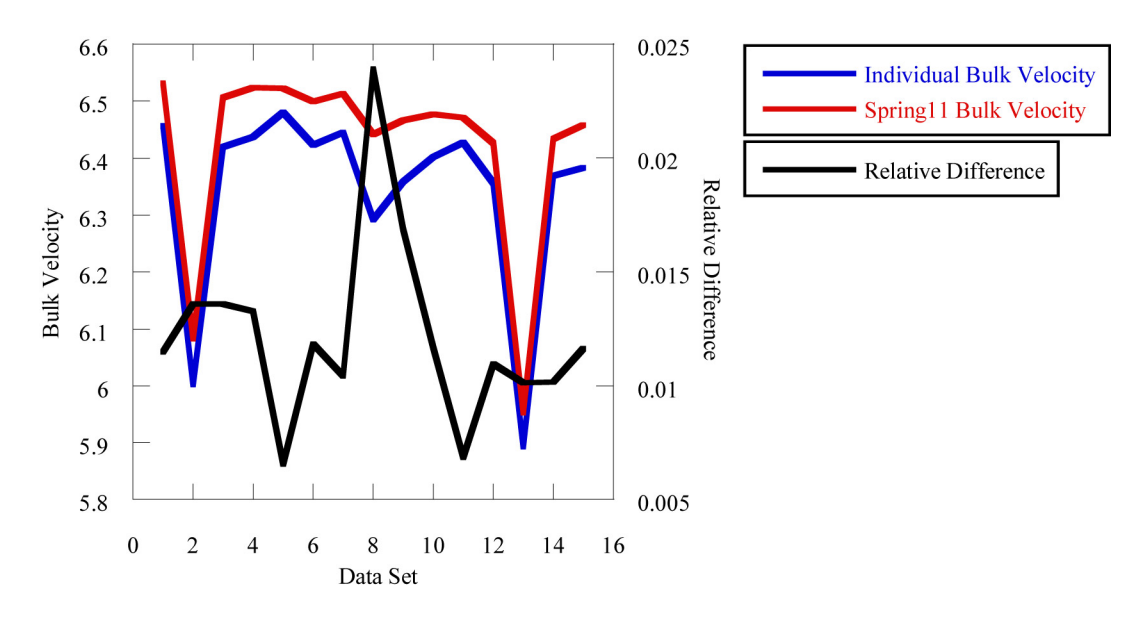


Figure 10: The bulk velocities found when the daily data is computed with the same calibration and mask versus the bulk velocity when the data is computed with an individual calibration and mask. The relative difference between the two velocity sets is also plotted. This relative difference is computed as the difference between the two velocities divided by the individual calibration velocity.

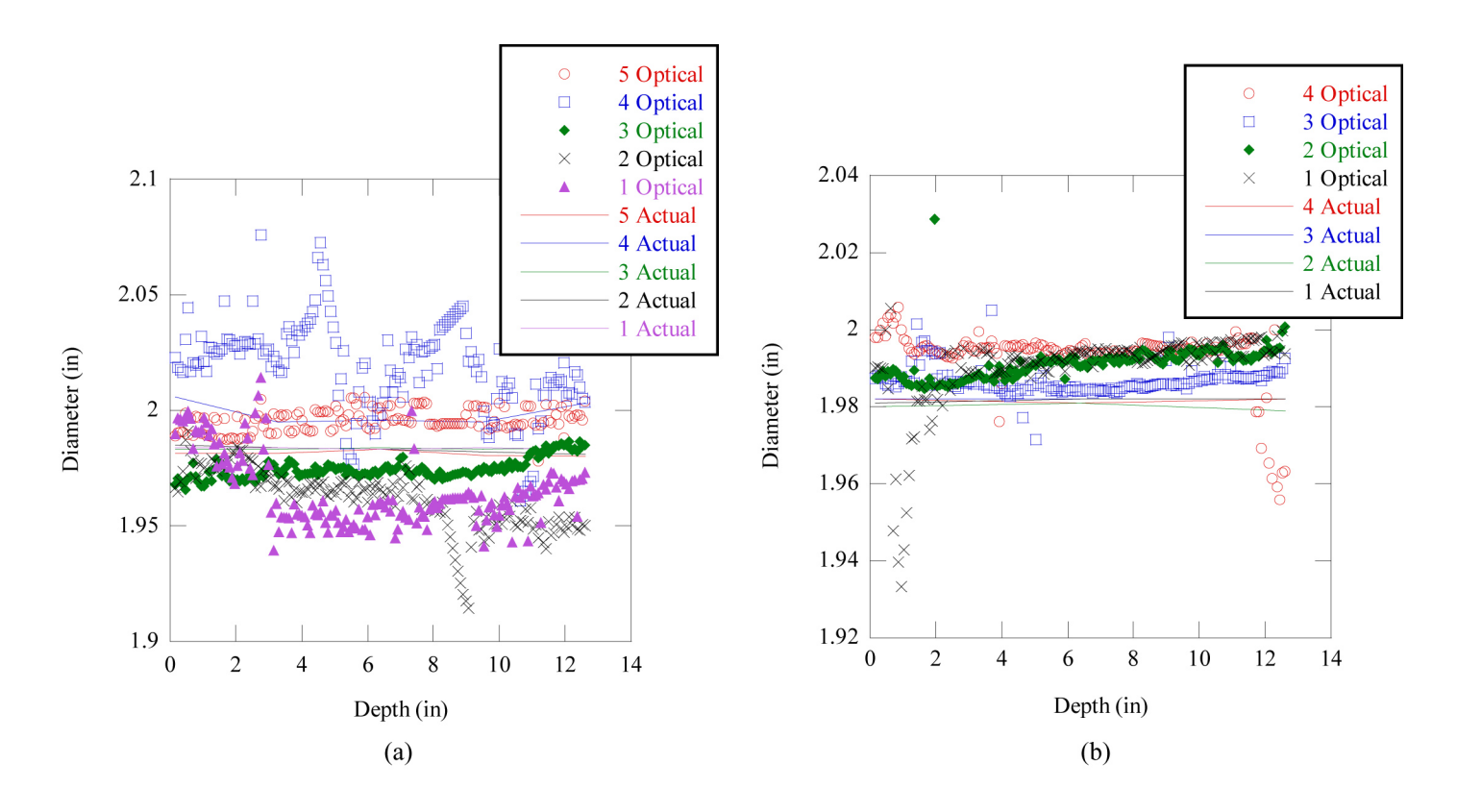


Figure 11: Diameter measurements of all (a) center cylinders and (b) bottom cylinders at various span wise locations using standard tools (solid lines) and measured optically (symbols).

The results from creating the solid model are also shown graphically in Fig. 12. Note the negative space is shown similar to what would be used in generating a mesh in a computational fluid dynamic (CFD) simulation. The solid model created in Gambit are taken exclusively from the optical data.

These results show that this approach is good for detecting cylinder misalignments. Even though this experiment was fairly lined up, a crooked cylinder is easily detectable as long as it is in the camera view. This is because of the nature of recording the intensity profile coordinate locations. However, this approach comes with a certain level of noise in the measurements. To use the raw data and solid model in a CFD simulation would incur errors at the surfaces due to inconsistencies that do not actually exist. To make this useful in CFD, the cylinders would need to be smoothed to a flat surface, such as by averaging or curve fitting the data points. These inconsistencies are due at least in part to the splicing of adjacent images. Improving the accuracy of the splicing points in successive images would reduce the noise in the results.

# 4 Conclusions

Experimental uncertainty is necessary when using the experimentally acquired data for validation purposes. This study was to determine the factors contributing to uncertainty of the cylinder array experiment and the resulting data. Velocity and pressure measurements were acquired daily for several months to find uncertainty contributors. Variance in atmospheric pressure varied the pressure drop readings, but not the bulk velocity in the channel. The velocity profile behind cylinder 4 did change from day to day, showing the large time scales that exist in the experiment. The repeatability uncertainty was of similar magnitude to the precision uncertainty for a data set and was correlated with the

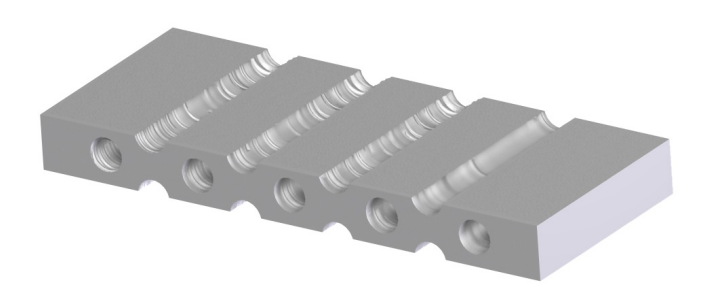


Figure 12: A solid model of the negative space of the test facility. The dimensions of this model are based solely on the optical measurements taken.

random wake mode switches. Adjustments to the camera and laser position increased the variation of the velocity profile behind cylinder 4.

As-built measurements were also performed on the array geometry. It was shown that for dimensions of the cylinders, direct measurements were more accurate, but the optical technique allows one to detect misalignment of components, of which the user may be unaware. The performance of the system was superior for a flat black surface (for which reflections were minimal) and was worst for a smooth, transparent surface. It is likely that the performance for transparent surfaces could be improved by not assuming that the intensity peak corresponds to the surface.

# References

- [1] W. L. Oberkampf and C. J. Roy. Verification and validation in scientific computing. Cambridge University Press, 2010.
- [2] B. L. Smith, J. J. Stepan, and D. M. McEligot. Velocity and pressure measurements along a row of confined cylinders. *J. Fluids Eng.*, 129(10):1314–1327, OCT 2007.
- [3] B. Wilson, J. Harris, B. L. Smith, and R. E. Spall. Validation of unsteady cfd in a confined row of cylinders. In *Proceedings of ASME Fluids Engineering Summer Conference*, July 2010. Paper number FEDSM2010-ICNMM2010-30720.
- [4] J. Hodson, R. E. Spall, and B. L. Smith. Turbulence model assessment for flow across a row of confined cylinders. *Nuclear Technology*, 161(3):268–276, 2008.
- [5] LaVision Inc. 301 W. Michigan Ave. Suite 403, Ypsilanti, MI 48197.